Electronic structure of metal hydrides. I. Optical studies of ScH_2, YH_2, and LuH_2

J. H. Weaver
Synchrotron Radiation Center, University of Wisconsin-Madison, Stoughton, Wisconsin 53589

R. Rosei*
Ames Laboratory United States Department of Energy and Department of Physics, Iowa State University, Ames, Iowa 50011

D. T. Peterson
Ames Laboratory United States Department of Energy and Department of Materials Science and Engineering, Iowa State University, Ames, Iowa 50011

(Received 30 November 1978)

We have examined the electronic structure of ScH_2, YH_2, and LuH_2 using optical absorptivity and thermoreflectance techniques in the photon energy range from 0.2 to 5 eV between 4.2 and 340 K. The measured quantities were used to determine the frequency-dependent dielectric functions and the dependence of the dielectric functions on temperature modulation. The results show that the low-energy properties ($h\nu \lesssim 1.5$ eV) are dominated by intraband absorption and a plasmon falling near 1.5–1.8 eV. Interband absorption is observed to be strong and structured above the interband onsets of ~ 1.25, ~ 1.6, and ~ 1.9 eV for ScH_2, YH_2, and LuH_2, respectively. The observed interband features can be interpreted in terms of the self-consistent band calculations of ScH_2 and YH_2 presented in the companion paper, and experimental features can be related to specific bands in particular parts of the Brillouin zone. The systematics observed in these three trivalent metal dihydrides can be correlated well to theory. Extensive studies with samples of varying hydrogen to metal ratio (x) within the dihydride phase were carried out to examine the influence of hydrogen sublattice disorder on the optical properties and electronic structure. It was observed that, for x approaching 2, interband features which could be related to d-band absorption were broadened by increasing lattice disorder, and new features in the interband absorption spectra were observed which could not be interpreted without postulating the hydrogen occupancy of significant numbers of octahedral sites. The strong x dependence of the optical features emphasizes the importance of studying well-characterized samples.

I. INTRODUCTION

Metal hydrides and metal-hydrogen systems have intrigued researchers ever since Graham first observed that Pd metal could absorb (occlude) large amounts of hydrogen.[1] The resulting literature of hydrides is voluminous with the PdH (PdD) system having undoubtedly been studied more than any of the others.[2] Today, hydrides are playing an increasingly important technological role, a role that certainly will increase as we move toward the postulated "hydrogen economy" and realize some of the numerous potential applications of hydrides. It is interesting and perhaps surprising that, although these systems have had a long and active technological history, many of the fundamental properties of H in metals remain rather poorly understood. For example, the nature of the chemical bond remains uncertain and controversial.

The technological need to characterize H in metals is responsible for a considerable amount of the recent activity. The discovery of such interesting properties as the enhanced superconductivity and inverse isotope effect[3-5] in PdH (PdD) has similarly lead to a redoubling of efforts aimed at revealing the fundamental physics and chemistry of metal hydrides.

Our recent interest in the hydrides has focused on the electronic structure as it can be examined through optical and photoelectron spectroscopy and through one-electron band-structure calculations. Preliminary measurements with ScH_2,[6] and NbH_x – TaH_x,[7] showed the feasibility of experimental optical studies and indicated that existing models of the electronic structure needed refining if quantitative agreement between theory and experiment was to be obtained. Indeed, although pioneering work had been done by Switendick,[8] many of those studying the various hydrides were still attempting to interpret experimental results through older, qualitative models (anion model, proton model, etc.). In our photoemission work with the thorium hydrides,[9] ThH_2 and Th_4H_{15}, we sought to show that the older models were inadequate to interpret the observed electronic structure and that additional calculations following Switendick's proposed model were in order.

In this paper, we discuss our optical studies of the dihydrides of Sc, Y, Lu and, by inference, the lanthanide dihydrides. In the companion paper,[10] self-consistent band calculations will be presented and the predictions of those calculations compared with experimental results. In this way, we shall show that there is excellent agreement between ex-

periment and one-electron band-model calculations for these dihydrides. It is hoped that these two papers, combining experiment and theory as they do, will serve to guide future thinking vis-á-vis the electronic properties of hydrides. In subsequent papers, we shall draw heavily on the background material presented here and, as a result, shall provide herein more detail regarding the experimental aspects than usual.

The outline of this paper is as follows: (i) introductory comments concerning hydrides and optical techniques; (ii) experimental technique and sample preparation; (iii) presentation of the data, data analyses, and discussion including x dependences. In the companion paper by Peterman *et al.*,[10] the discussion will be extended and the interpretation of interband features based on concurrent calculations made more quantitative.

As we shall show in the present paper, there are several aspects of these dihydrides that are important and revealing as far as the electronic structure is concerned.

The low-energy absorptivity spectra show that the dominant absorption mode is intraband for $h\nu \leq 1$ eV and a sharp plasmon edge occurs in the near infrared (1.4–1.9 eV). This edge and the character of subsequent interband absorption, which becomes increasingly important above about 1.5 eV, govern the physical appearance of these materials: they are dark with colors ranging from grey for ScH_2 (low, nearly constant reflectance in the visible) to blue for LuH_2 (the magnitude of the reflectance changes significantly in the visible).

Thermoreflectance spectroscopy makes it possible to emphasize transitions involving Fermi-surface states and critical points; as we will show, these are important for the dihydrides, more important than has been found to be the case for metals themselves which tend to have structures formed from volume effects rather than critical points.[11,12] Such results make it possible to be quantitative in our comparison with the predictions of theory.

Studies with samples with different compositions or x values ($x = H/M$ ratio as in ScH_x, for example) have shown that the interband features between ~1.5–2 and 5 eV (our high-energy limit) can be related to the relatively localized, d-derived states, i.e., they show little dependence on hydrogen sublattice vacancies. Further, the results with samples of various concentrations indicate that there remains some uncertainty as to the kind of interstitial site occupied as $x \to 2.0$. In particular, we find that YH_x has electronic structure which can be interpreted very well by the calculations of YH_2 only for lower values of x near 1.7 (close to the dihydride phase boundary). For x approaching 2.0, additional interband structures appear at low energy, which cannot be related to dihydride band states since the band structure reveals no possible interband transitions near 0.5–1 eV. We tentatively attribute this behavior to the occupation of octahedral interstitial sites and appeal for further corroborating studies.

II. PRELIMINARY COMMENTS

A. Metal hydrides

The recent observation that the addition of H to a metal can enhance the superconducting transition temperature T_c contradicted the conventional wisdom and served to motivate a considerable amount of fundamental research (both experimental and theoretical); the PdH and PdD systems, with $T_c(\mathrm{PdH}) < T_c(\mathrm{PdD})$, have been the most intensively studied.[3-5] Other intense efforts have involved technological applications related to hydrogen storage (the density of interstitial H in a metal lattice can exceed that of H in liquid or solid H) and hydrogen embrittlement (in general, the absorption of H causes the normally ductile metal to be brittle). Some of these and other intriguing features of hydrides have recently been discussed by Westlake, Satterthwaite, and Weaver.[13]

In our present study of Sc-group dihydrides (including the lanthanides as part of that group), we consider those dihydrides which crystallize in the fcc CaF_2 structure shown in Fig. 1. As can be seen, the metal sites define the fcc lattice with interstitial hydrogen occupying tetrahedral sites (shown) or octahedral sites (not shown). In principle, the dihydrides with $x = 2$ would have completely occupied metal and hydrogen sublattices; vacancies would appear in the tetrahedral hydrogen sublattice for $x < 2$ and octahedral sites would be fil-

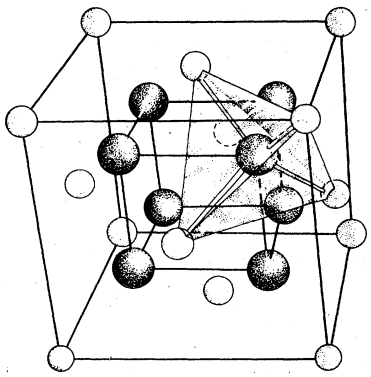

FIG. 1. Crystal structure of the CaF_2 fcc dihydride. The metal atoms occupy the fcc sites and proton occupies the tetrahedrally coordinated sites as shown. Octahedral sites are not shown but correspond to positions halfway between metal atoms on the cube edge.

led for $x > 2$. In practice, the minimum energy configurations of the various systems inhibit or enhance modifications of this simple scheme,[14] some systems (TiH_2 for example) exhibiting tetragonal distortions for x approaching 2 and others seeming to allow simultaneous tetrahedral and octahedral occupation for $x < 2$. Switendick[8] has discussed some aspects of the problem, but a complete and comprehensive model has not yet been formulated.

Metal hydrides can be prepared in a variety of different ways including ion implantation, electrolytic charging, and charging from the gas phase. A summary figure showing the metals which do form hydrides and the structure of each can be found in Ref. 13; other detailed information can be found in several reviews of hydrides.[2,14]

To date, there have been relatively few hydrides that have been prepared as single crystals; exceptions include NbH_x (NbD_x), CeH_x, and PdH_x. Some hydrides are relatively unstable and will decrepidate when exposed to laboratory air (e.g., YH_2 will blister when exposed to moist air; LaH_2 will quickly be reduced to finely divided powder). Others such as ScH_2 and LuH_2 are very stable.

B. Optical spectroscopies

The reason for our interest in optical spectroscopies is that the quantity which is determined [the complex dielectric function $\tilde{\epsilon}(\omega)$] reveals the character of the electronic band structure, i.e., structure in the dielectric function can be related to $\vec{k}$-conserving electric dipole interband transitions from an initial state $|i\rangle$ to a final state $|f\rangle$ separated by an energy $h\nu$. In the low-energy range before the onset of interband absorption, the dielectric function reveals the characteristics of intraband absorption (relaxation time, plasma frequency, static lattice dielectric constant). Since optical techniques directly probe the electronic states, they give results which can be compared to first-principles band calculations through

$$\omega^2\epsilon_2 = \frac{e^2\hbar^2}{3\pi m^2}\sum_{i,f}\int_k d^3k\,|\langle i|p|f\rangle|^2 \times \delta(E_f(\vec{k}) - E_i(\vec{k}) - \hbar\omega). \quad (1)$$

Hence, the approximations and assumptions underlying a band calculation can be tested by comparing the predictions of Eq. (1) with experimental results.

In this paper, the results of two different kinds of measurements will be used to gain insight into the electronic structure of dihydrides. These are static absorptivity measurements and modulated thermoreflectance measurements. In the first, the dielectric function of the static system is determined by measuring the absorptivity (or reflectance since $A = 1 - R$) then computing the dielectric function $\tilde{\epsilon} = \epsilon_1 + i\epsilon_2$; structure in ϵ_2 can then be compared to the predictions of band theory [i.e., Eq. (1)]. In the modulation measurements, additional band-structure information is obtained by modulating one of the parameters of the system, temperature in the present case, and comparing the results with predicted dependence of $\tilde{\epsilon}$. Thermomodulation also makes it possible to examine plasmon modulation and assess the importance of modulation of the broadening parameter and the plasma frequency.

In the static absorptivity measurements, A (or R) is measured as a function of photon energy. R can be defined as $R = \tilde{r}\tilde{r}^* = I/I_0$ or the ratio of incident to reflected light intensities; $\tilde{r} = re^{i\phi}$ is the reflectance coefficient and ϕ is the phase shift of the reflected wave relative to the incident wave. Further, $\tilde{r} = (\tilde{N} - 1)/(\tilde{N} + 1)$, $\tilde{\epsilon}(\omega) = \tilde{N}\tilde{N}^*$, and the dielectric function can be determined algebraically once R and ϕ are known. R can be measured directly and ϕ can be determined through Kramers-Kronig analysis, viz.,

$$\phi(\omega_0) = \frac{2}{\pi}\int_0^\infty \frac{\ln R(\omega)}{\omega^2 - \omega_0^2}\,d\omega. \quad (2)$$

Hence, from our measured reflectance (or absorptivity) spectrum, we can calculate ϕ and determine ϵ_2 for comparison with theory.

In the modulation measurements, we are more interested in changes in R (and hence changes in $\tilde{\epsilon}$) than in the static quantities. In our thermoreflectance measurements, we hoped to emphasize critical point and Fermi-surface transitions, for example. These interband transitions have well-defined line shapes in $\Delta R/R$ (the measured quantity) and in $\Delta\tilde{\epsilon}$ (the determined quantity), and the spectra can be compared with predictions from theory.

An ideal comparison between theory and experiment involves a computation of Eq. (1). Generally, Eq. (1) is simplified by assuming the matrix elements are slowly varying functions of $\vec{k}$ and do not introduce structure (though they might distort structures). Under that assumption, Eq. (1) is proportional to the joint density of states (JDOS) and emphasizes the geometric character of pairs of bands. Structure in the JDOS can be compared to experiment; e.g., two bands which are parallel over an appreciable volume of $\vec{k}$ space have a large JDOS and might be responsible for structure in ϵ_2.

In the remainder of this paper, we will discuss the experimental aspects of determining $\tilde{\epsilon}$ and $\Delta\tilde{\epsilon}$. In the companion paper,[10] calculations of the band structure, the JDOS, and simulated thermo-

modulation of the bands will be presented and compared with the experimental results. As will be seen, the agreement is excellent.

III. EXPERIMENTAL TECHNIQUES

The reflectance of a material R can be determined by measuring the intensities of the incident and the reflected photon beams; alternatively, the absorbed and reflected beams can be measured to determine the absorptivity $A = 1 - R$. The latter technique has the advantage that when R approaches unity, as it does for metals in the infrared, a measurement of A to 1% of A is more precise than a measurement of R to 1% of R. For the measurements discussed here, we have determined A at near-normal incidence, 4.2 K, between 0.2 and 4.4 eV.

The technique employed here has been termed calorimetry because it makes use of the temperature increase of the sample which results from the absorption of radiation. Briefly, the sample is illuminated by monochromatic light, some fraction of the light is absorbed by the sample and the remainder is absorbed by a Au-black-coated absorber. Both the sample and absorber are at 4.2 K and, because of their low heat capacities, both are heated (mK) when illuminated. By interrupting the radiation and duplicating the temperature increase of each element through joule heating, it is possible to determine the energy absorbed by each element (μW) and hence the absorptivity. Further details of the experimental procedure can be found in Ref. 15.

The details of the thermoreflectance technique can also be found elsewhere,[12] but a few points should be reiterated here. The measurements were conducted at near-normal incidence between 0.5 and 5 eV using PbS and photomultiplier detectors. The sample was in thermal contact with a thin-film Cr heater which was pulsed at 2 Hz. The resulting temperature variation at the sample surface (a few Kelvin) produced the modulation in the reflectance. This ac signal was measured with lock-in amplifier techniques. Signals of parts in 10^4 were detected with accuracies of better than 5%. The ambient temperature of the sample was varied by changing the cryofluid (liquid N_2, dry ice plus acetone, or ice water) and/or the rms power dissipated in the heater. For the measurements reported here, the ambient temperature of the sample was $\simeq$140 K or $\simeq$340 K.

IV. SAMPLE PREPARATION

The preparation of well-characterized specimens of metallic hydrides requires considerable care. The large effects of impurities in the starting metals and the wide stoichiometry range of many of these compounds can lead to marked differences between nominally similar compositions. The available information on the phase diagrams is usually incomplete and sometimes wrong or contradictory. Surface layers of metal oxides or other compounds may make exchange of hydrogen with a hydrogen gas pressure depart markedly from equilibrium at temperatures below 875 K. This surface resistance to the transfer of hydrogen can be a particular problem when dealing with hydride powders as it allows the individual particles to deviate widely from the average concentration of the specimen and these composition differences are not removed by heating to moderate temperatures.

All of the samples used in our studies were bulk samples prepared from high purity polycrystalline metal obtained within the Ames Laboratory U. S. Department of Energy. These metals contained less than 5 ppm of any metallic impurities and typically about 30 ppm oxygen, 5 ppm nitrogen, and 10 ppm carbon. The metals were electropolished to leave a clean surface, wrapped in 0.05 mm-thick tantalum foil and heated under vacuum in the charging apparatus to 1125 K to outgas the specimen and to increase the surface permeability to hydrogen. The tantalum foil wrapping prevented contamination of the specimen by the Vycor or stainless-steel furnace tubes. Also, the tantalum foil allowed hydrogen to pass through readily but would react with carbon and oxygen bearing gases before these could contact the specimen. Pure hydrogen from thermal decomposition of UH_3 was used for the charging runs at one atmosphere hydrogen pressure or below. The charging runs that used higher hydrogen pressures up to 100 atmospheres were made with special purity tank hydrogen. The temperature and hydrogen pressure were chosen, based on the pressure composition data reported in Mueller, Blackledge, and Libowitz,[14] so as to give the desired hydrogen concentration. The sample was then cooled quickly by removing the furnace so as to reduce the amount of additional hydrogen absorbed during cooling. A given set of charging conditions did not always produce hydrides of the same hydrogen concentration. Specimen size and the time at temperature had an influence on the concentration that was obtained. In all cases, however, the concentration within a single hydride specimen was always uniform and no evidence of concentration gradients within a specimen were observed by optical metallography or by hydrogen analysis.

The hydride phase composition limits are all wider at higher temperatures than at low temperature and so there may be precipitation of either hydrogen-saturated metal phase or of the metal tri-

TABLE I. Lattice constants of ScH_2 and YH_2 at several compositions.

Composition	Lattice constant, (Å)
$ScH_{1.61}$ [a]	4.782
$ScH_{1.88}$	4.783
$ScH_{1.98}$	4.783
Mueller, Blackledge, and Libowitz	4.784
$YH_{1.47}$ [a]	5.207
$YH_{1.73}$ [a]	5.208
$YH_{1.91}$	5.207
$YH_{1.96}$	5.204
$YD_{1.88}$	5.195
Mueller, Blackledge, and Libowitz	5.199–5.209

[a] MH_x + metal phases.

hydride during cooling. The specimens were always examined by optical metallography to determine whether one or two phases were present. The grain size of the hydride phase was usually quite large with individual crystals up to several millimeters across. The hydrogen concentration of the specimens was determined by a hot-vacuum-extraction method. The hydrogen was pumped from a weighed sample at 1225 K into a calibrated volume. The accuracy and precision of this analytical technique is about one relative percent.

X-ray diffraction Debye patterns were used to obtain the lattice constants of the hydride compositions. The data in Table I show that there is no change in the lattice constant of ScH_2 and only a small change in YH_2 over the indicated composition range.

The specimen surfaces were prepared for the optical measurements by wet grinding one surface flat with 600 grit abrasive paper. This surface was then polished by hand with Linde *A* abrasive (0.3 μm alumina) on a rotating wax wheel. These hydrides are quite hard and this polishing procedure produced flat surfaces with very little strain or structural damage. Most of these metal dihydrides of the Group-VII *B* and lanthanide metals cannot be electropolished successfully. The lutetium hydride sample was electropolished in a perchloric-acid–methanol electrolyte at 200 K and this surface gave essentially the same absorption curve as the abrasive prepared surface. ScH_2 and LuH_2 are relatively inert to ambient moisture and will remain unchanged in appearance for several months when exposed to air. YH_2 is much more sensitive, however, and after a few hours will show surface eruptions and decrepitation, so it was stored under argon.

The samples used in the calorimetric measurements were typically 8×12×2 mm; those used for the thermoreflectance were much smaller (2×3×0.1 mm) so that their thermal mass was small and the time constant of the sample was compatible with 2-Hz modulation. In all cases, the samples were mechanically polished, then transferred to the experimental chamber and sample holder, and evacuated. The measurements themselves were conducted at 4.2 K (calorimetry) or ~140 K and ~340 K (thermoreflectance).

The measurements reported here involve samples of ScH_x with $1.61 \leq x \leq 1.98$; YH_x with $1.73 \leq x \leq 1.96$; YD_x with $x = 1.88$; and LuH_x with $1.83 \leq x \leq 1.98$. These results extend over the range of composition of the dihydride phase as reported in the literature.[14] As we will show, the optical measurements are an excellent means of identifying the deviation from purely tetrahedral occupation for YH_2, and we will suggest that for x approaching 1.9 or greater, there are significant octahedral sites occupied.

V. RESULTS AND DISCUSSION

The measured optical absorptivities of ScH_2, YH_2, and LuH_2 are shown in Fig. 2. For visual clarity, the results for ScH_2 and YH_2 have been displaced upward and the horizontal lines extending from the left represent the respective zeros.

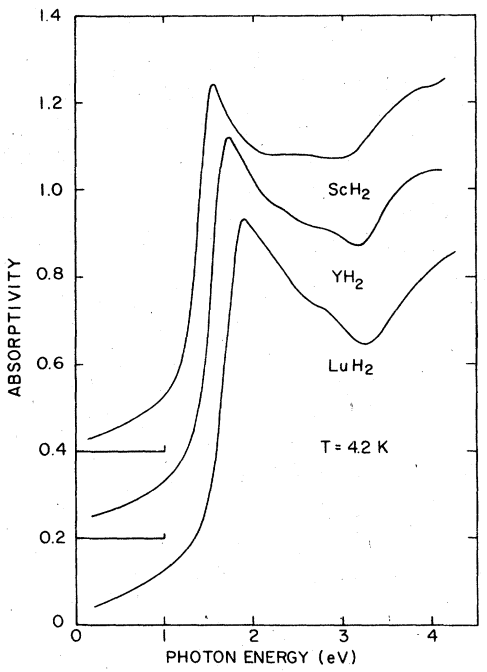

FIG. 2. Optical absorptivity of ScH_2, YH_2, and LuH_2 at 4.2 K and near-normal angle of incidence. The results for ScH_2 and YH_2 have been displaced upward for clarity. The results shown are for samples with hydrogen concentrations of $ScH_{1.61}$, $YH_{1.73}$, and $LuH_{1.83}$.

The H-to-M ratios of the samples shown in Fig. 2 are $x=1.61$ for ScH_2, $x=1.73$ for YH_2, and $x=1.83$ for LuH_2. These samples are single phase dihydrides as determined through microscopic examination and x-ray analyses. Comparison of the composition with phase diagrams from the literature indicates that the samples lie close to the terminus of the dihydride phase. For these samples, then, we can expect that the hydrogen occupies only tetrahedral sites and 8% (LuH_2) to 20% (ScH_2) of those sites are vacancies. As we shall argue in the next paragraphs, the results shown in Fig. 2 are the most representative of the dihydrides because samples closer to stoichiometry (H-to-M ratio of 2) can have octahedral hydrogen as well as tetrahedral hydrogen. After first discussing our studies of the x dependence of the absorptivity of ScH_2 and YH_2, we shall return to the results of Fig. 2 for detailed data analysis and interpretation.

A. Concentration dependence

The dependence of the electronic structure on stoichiometry has been an interesting (and complicated) problem that has confronted those studying interstitial alloys in general (e.g., carbides, nitrides, oxides, sulfides). It was our feeling when these hydride studies were undertaken that they offered a unique opportunity to examine the x dependence of the electronic structure and to relate changes to disorder-induced broadening of the band states. These hydrides have metal sublattices which are nearly perfect and hydrogen sublattices which can tolerate ~20% vacancies. It had been predicted that band states for $x \simeq 2$ would have well-defined eigenenergies but that, when x deviates from 2, those energies would broaden if the corresponding wave functions sampled the disorder by having appreciable amplitude at the (hydrogen) disorder site.[16] States that are more localized, such as the d-derived states, would be less sensitive to broadening. Hence, optical transitions involving the d states would not change significantly while those involving H-derived s-like states would have large x dependences.

The results for studies of ScH_x ($x=1.61$ and 1.98), YH_x ($x=1.73$ and 1.96), and LuH_x ($x=1.83$ and 1.98) are shown in Fig. 3. Not shown are the analogous spectra for samples of $ScH_{1.81,1.88}$, $YH_{1.88,1.93}$, and $LuH_{1.93}$. As can be seen, the structures in the absorptivity spectra above the maxima near 1.8 eV are less sensitive to concentration than are those at lower energy. Changes in the higher energy features reflect a broadening or reduction in sharpness which accompanies the approach to stoichiometry of a H-to-M ratio of 2.0. Those results suggest that the interband features

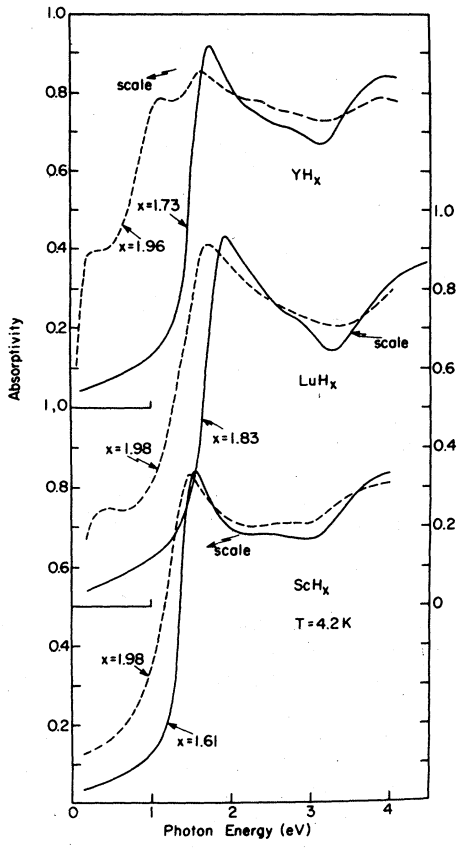

FIG. 3. Optical absorptivity of ScH_X, YH_X, and LuH_X showing the x dependence of the absorptivity. For ScH_X, the magnitude of the absorptivity increases but shows no structure at low energy. For LuH_2, the background increases and a clearly defined interband feature develops near 0.4 eV. For YH_X, there is a progressive increase in the magnitude of the structure near 0.3 and 1.1 eV for increasing x. These low-energy structures are tentatively interpreted as due to occupation of octahedral sites. Measurements of YD_X show the same behavior and no isotope effect.

are due to interband transitions involving d-derived states and that the disorder in the lattice *increases* instead of decreases for $x \to 2$.

The results shown in Fig. 3 show that the optical properties change very markedly with x in the energy range below 1.8 eV. For ScH_x the absorptivity increases at low energy and the maximum shifts to lower energy for x increasing from 1.61 to 1.98. For LuH_x, the same increase in magnitude is observed, the peak again shifts to lower energy, but a new low-energy structure near 0.5 eV is also seen to appear for $x=1.83 \to 1.98$. For YH_x, not only does the magnitude increase and the peak shift but first a structure near 0.4 eV grows and then is joined by the "bite" near 1.25 eV. The extreme spectra are shown in Fig. 3 but the development of those features can be seen in the samples

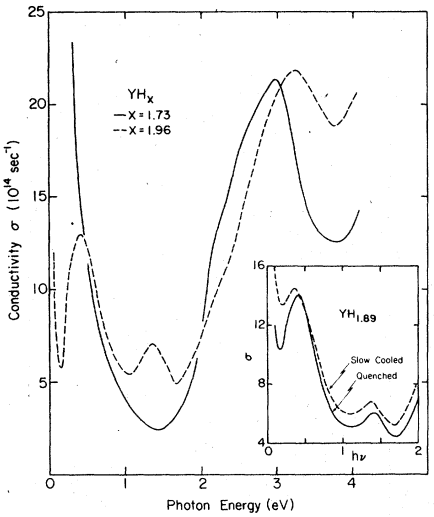

FIG. 4. Optical conductivity spectra of $\sigma = \epsilon_2 E/4\pi\hbar$ for $YH_{1.73}$ and $YH_{1.96}$ show the strong x dependence of the optical properties of YH_x. For $x \to 2$, the two prominent features at low energy appear and the interband features at higher energy are broadened. In the inset, the results for slow-cooled and quenched $YH_{1.89}$ are shown; quenching has the effect of freezing in more octahedral-site hydrogen.

with intermediate hydrogen concentrations.

The sensitivity of these low-energy structures to hydrogen concentration indicates that hydrogen-induced states participating in the interband absorption are very near the Fermi energy. In the band structure of YH_2 one would then expect to see hydrogen-derived states close to E_F. However, as is discussed by Peterman *et al.* in the companion paper, there are no bands in CaF_2-structured YH_2 that could account for these states. Instead, the hydrogen occupation of octahedral sites is shown to be a plausible explanation.

The tendency of hydrogen to occupy octahedral sites should show a dependence on the size of the octahedral hole or equivalently the lattice constant. For the three dihydrides under discussion here, the lattice constant increases from about 4.78 Å in ScH_x to 5.03 Å in LuH_x to 5.2 Å in YH_x. As can be seen in Fig. 3, the appearance of the low-energy "octahedral" structure follows the same trend: though the absorption increases in ScH_x, there is no observed structure; structure is observed in LuH_x near 0.5 eV; and two features are observed in YH_x near 0.35 and 1.25 eV.

To test the hypothesis of octahedral site occupation, we first prepared a sample of $YH_{1.89}$, slowly cooled it from 500 °C, and measured the absorptivity spectrum as usual. The sample was then reheated in argon to 500 °C and quenched in ice water to freeze in a higher concentration of octahedral hydrogen. The absorptivity spectrum for that quenched sample showed the structures at 0.5 and 1.25 eV to grow from shoulders to well-defined features more nearly like the spectrum shown in Fig. 3 for $x = 1.96$. Those results are consistent with the octahedral site occupation proposed here. In Fig. 4, the optical conductivity spectra, $\sigma = \epsilon_2 E/4\pi\hbar$, for $YH_{1.89}$ quenched and slow cooled are shown to make the point clearly (the discussion of the derivation of ϵ_2 or σ will follow in Sec. V B). Clearly, then, one must know not only the bulk H-to-M ratio but also the history of the sample. The implication is that studies which are sensitive to the electronic structure (specific heat, magnetic susceptibility, Compton profile, etc.) must take into account the deviation of the sample from purely tetrahedral-dihydride character.

In a subsequent paper, we shall discuss the results of additional calculations beyond those presented in Ref. 10 and will present the results of studies of dihydride-trihydride systems that allow for higher concentrations of hydrogen, i.e., for $1.8 \leq x \leq 3$, with no crystal structure change. There remains a considerable amount of work to be done before x dependences can be understood and the character of these hydrides can be considered known.

Optical absorptivity measurements have also been performed with a sample of $YD_{1.88}$ to examine any isotope effect. Those results showed that, within the uncertainty in preparing identical samples of hydride and deuteride, the deuteride possessed the same low energy (O-T) structure; above 2 eV, the interband features were practically identical to those of the dihydrides. The differences which are observed can be understood in terms of sample preparation. The temperature of charging, the rate of cooling, and the hydrogen pressure must influence the degree to which O sites are occupied; to our knowledge, however, there has been no systematic study of these parameters.

For the remainder of this paper, we shall emphasize the results shown in Fig. 2, the quantities derived from them, and thermoreflectance results with the same samples.

B. Low-x dihydrides

The absorptivity spectra for the low-x samples of ScH_2, YH_2, and LuH_2 are shown in Fig. 2. For each dihydride, the absorptivity rises smoothly and without structure as $h\nu$ increases above 0.15 eV (our low-energy limit). The absorptivity of each has a sharp edge (maximum slope near 1.37 eV for ScH_2, 1.53 eV for YH_2, and 1.73 eV for LuH_2) with A reaching ~0.90 at the maximum. The absorptivity spectra above the edge are qualitatively similar for each dihydride. The strength of the

absorption minimum near 3 eV can be seen to increase for ScH_2 to YH_2 to LuH_2 (Fig. 2). The systematic increase in that feature accounts for the characteristic physical appearance of these dihydrides. That is, the reflectivity for ScH_2 (which is dark grey) is nearly constant from 2 to 3 eV while that of LuH_2 (which is deep blue) is nearly four times as great at 3 eV as at 2 eV. The other lanthanide dihydrides have analogous features.[17]

A comparison of the optical results for these dihydrides with the analogous spectra for the metals Sc, Y, and Lu (Ref. 18) shows how radically different the optical properties, and hence the electronic structure, of the dihydrides are from those of the metal. In particular, the low-energy optical properties of the dihydrides reflect intraband absorption and the plasmon edge near 1.5 eV; the low-energy optical properties of the hcp metals are strongly anisotropic and are dominated by interband absorption. The results of Fig. 2 (dihydrides) and Ref. 18 (pure metals) show that any attempt to rearrange the bands of the metal to account for hydrogen-induced changes would be doomed to failure: These hydrides cannot be viewed as "metal-like"; ScH_2 is not "like" Sc metal.

As was discussed in Sec. III, the interpretation of the optical results can best be made through considerations of the dielectric function, $\tilde{\epsilon}$. The Kramers-Kronig integral [Eq. (2) above] was used to determine $\tilde{\epsilon}$. The results of Fig. 2 (0.15–4.4 eV) were extended to zero and infinite energies to satisfy the limits on the integration. The infrared extrapolation was determined by fitting the absorptivity spectra between 0.15 and 1 eV with Drude parameters, then using those parameters at lower energy. The extrapolation to 25 eV was guided by unpublished[19] reflectance spectra ($2.5 \leq h\nu \leq 25$ eV), then extended to 10^4 eV by assuming that the core level absorption of the dihydrides would qualitatively resemble those of the metals themselves. This latter assumption, although not completely valid, allowed us to satisfy the sum rules on the dielectric function.

The results of the Kramers-Kronig analyses are shown in Fig. 5 for the low-x dihydrides of Sc, Y, and Lu. The dielectric functions reflect the similarities of these dihydrides as observed in Fig. 2. In each case, the low-energy behavior is dominated by intraband or Drude absorption. This accounts for the large but monotonically decreasing magnitudes of ϵ_2 and the large, negative, decreasing behavior of ϵ_1. For ScH_2, the Drude behavior is extended semiquantitatively (dashed line) into the region where interband absorption is dominant; also shown is the interband onset near 1.2 eV.

The intraband region of absorption can be treated quantitatively because $\tilde{\epsilon}$ can be calculated within

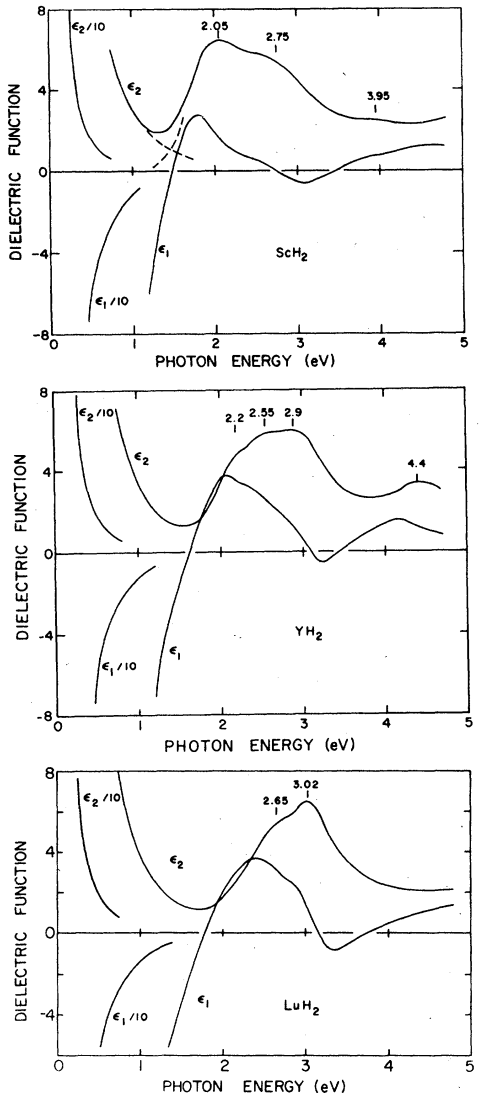

FIG. 5. Dielectric functions for $ScH_{1.61}$, $YH_{1.73}$, and $LuH_{1.83}$ as derived from the results of Fig. 2. Below about 1.5 eV, the dielectric function is dominated by Drude absorption; at higher energy, interband effects are responsible for the increased absorption and structure. For ScH_2, the interband onset is sketched semiquantitatively.

the framework of the Drude model, namely,

$$\tilde{\epsilon}(\omega) = \epsilon_s - \omega_p^2/\omega(\omega - i/\tau), \tag{3}$$

where τ is the electronic relaxation time (or reciprocal phenomenological broadening parameter $\Gamma = i/\tau$), ϵ_s is the static dielectric function, and ω_p is the plasma frequency. Analyses of the dielectric functions of Fig. 5 give the following Drude parameters for the samples studied: ScH_2: $\hbar\omega_p = 4.1$ eV; $\epsilon_s = 5.6$; $\tau/\hbar = 8.7$ eV^{-1}; YH_2: $\hbar\omega_p = 4.09$ eV; $\epsilon_s = 4.8$; $\tau/\hbar = 7.0$ eV^{-1}; LuH_2: $\hbar\omega_p = 4.4$ eV; $\epsilon_s = 5.2$;

$\tau/\hbar = 5.2$ eV^{-1}. These parameters describe the behavior of the dielectric function below the onset of interband absorption (less than 1.0–1.5 eV) and were determined by plotting ϵ_1 vs ω^{-2} and $\epsilon_2\omega$ vs ω^{-2}. Though they are useful in describing the infrared behavior, some caution must be employed because we have observed that the optical properties, and hence the Drude parameters, of these dihydrides are x dependent.

The plasmon behavior can be examined through the volume loss function, $\mathrm{Im}(-1/\tilde{\epsilon})$, which represents the probability that a propagating energetic electron will excite a volume plasmon. For a Drude system free of interband absorption, the plasma frequency corresponds to the energy at which ϵ_1 passes through zero. In a system in which interband absorption can overlap the region of the intraband absorption, the plasmon will be hybridized and screened (low-energy dispersion in ϵ_1 due to interband absorption will shift the zero crossing of ϵ_1—see Dietz *et al.* in Ref. 20 for a discussion of screened plasmons).

The loss functions for our dihydride samples have been calculated from the dielectric functions and are shown in Fig. 6. As can be seen, a sharp peak is observed at 1.78 eV for $LuH_{1.83}$, 1.64 eV for $YH_{1.73}$, and 1.47 eV for $ScH_{1.61}$. As was shown in Ref. 6, the shape of that loss function peak can be approximated by a Lorentzian and deviations can be related to interband absorption which accounts for the increasing backgrounds in $\mathrm{Im}(-1/\tilde{\epsilon})$ and the structure in $\tilde{\epsilon}$.

The spectra in Fig. 6 for $ScH_{1.98}$ and $ScH_{1.61}$ reveal the effects on the loss function of weak, structureless interband absorption which occurs near $\hbar\omega_p$ and increases for $x \rightarrow 2$ (octahedral effects). The plasmon peak is seen to shift from 1.47 eV for $x = 1.61$ to 1.39 eV for $x = 1.98$ and broaden (full-width at half-maximum increases from 0.21 to 0.30 eV). This shift is in contrast to what should be observed for a simple Drude system in which the plasma frequency would shift toward higher energy as $\sqrt{x}$. The results for LuH_x show the analogous broadening of the plasmon and a greater shift toward lower energy. For LuH_x, the shift can be related to low energy dispersion in ϵ_1 and ϵ_2 due to the weak interband absorption near 0.4 eV. The results for YH_x show the effects of strong interband absorption near ~0.3 and 1.3 eV which is "turned-on" as the hydrogen-to-metal ratio approaches 2.0. The plasmon is screened by low-energy interband absorption and is dominated by the interband structure in $\mathrm{Im}(-1/\tilde{\epsilon})$ at 1.05 eV in $YH_{1.96}$.

Thermoreflectance studies were undertaken to learn more about the low-energy plasmons and the interband features. The results of those studies

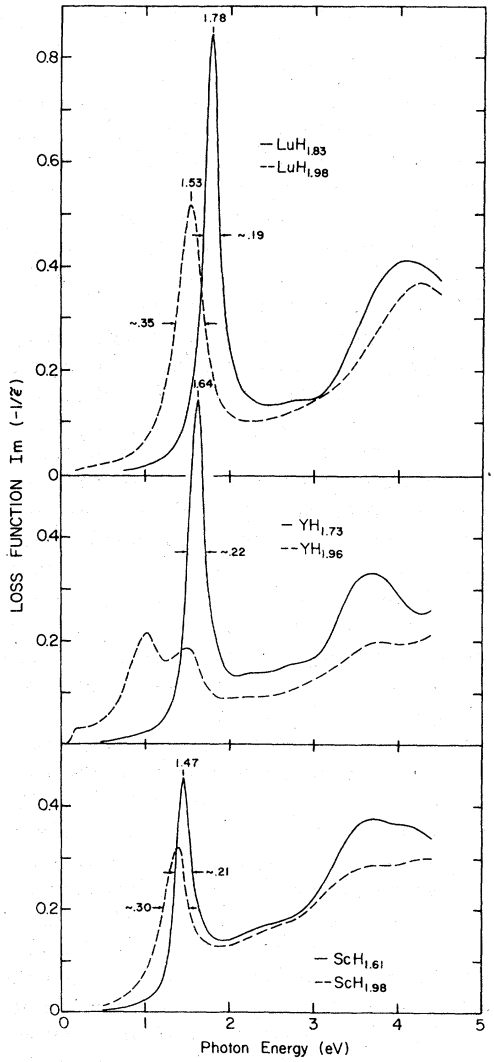

FIG. 6. Loss function for ScH_x, YH_x, and LuH_x calculated from the results of Fig. 5. Each dihydride exhibits a strong low-energy plasmon, and the effects of stoichiometry on the plasmon are shown. For $ScH_{1.98}$ the plasmon is shifted slightly and broadened. For $LuH_{1.98}$, it is shifted by the weak interband structure near 0.4 eV and broadened. For $YH_{1.96}$, the strong "octahedral" interband absorption accounts for the severe distortion of the plasmon structure and for the features at about 0.3 and 1.1 eV.

of low-x ScH_2, YH_2, and LuH_2 are shown in Fig. 7. For convenience, the thermoreflectance spectra $\Delta R/R$ are shown with arbitrary units. The thermoreflectance magnitudes were typically a few parts in 10^3 and scaled with the temperature excursion ΔT of the sample. As usual, ΔT was controlled by experimental conditions such as the efficiency of thermal coupling of sample to heater, the rms power dissipation, and the modulation frequency. For our work, $\Delta T \simeq 3$–5 K and $T \simeq 140$ K.

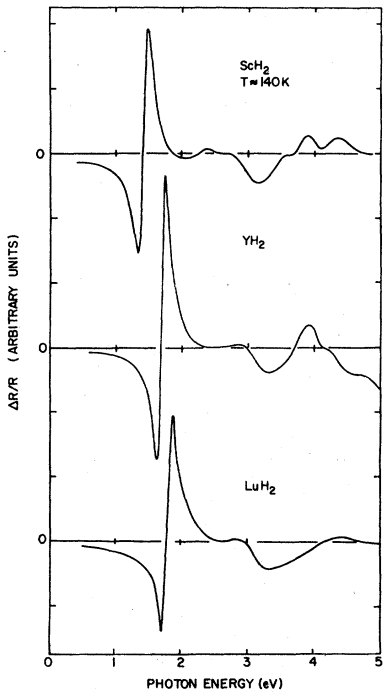

FIG. 7. Thermoreflectance spectra of $ScH_{1.61}$, $YH_{1.73}$, and $LuH_{1.83}$ at about 140 K with bulk samples. The lowest-energy feature is interpreted as due to mixed plasmon and interband modulation while the higher-energy features reflect interband temperature modulation. $YH_{1.73}$ has a very weak structure at 2.45 eV, which is not visible on this scale; the corresponding structure is stronger in $ScH_{1.61}$ but not observed in $LuH_{1.83}$.

The spectra of Fig. 7 again reveal the similarities in the electronic structure of these dihydrides. The dominant structure in each is the low energy, derivativelike feature near 1.5–1.8 eV. A measure of the width of that structure can be taken as either the separation at half maximum of the positive and negative lobes (350–400 meV) or as the energy separation of the positive and negative peaks (147 meV for LuH_2, 125 for YH_2, and 140 for ScH_2). The zero crossing of $\Delta R/R$ occurs at 1.41 eV for ScH_2, 1.675 eV for YH_2, and 1.791 eV for LuH_2 at 140 K. The proximity of this structure to the volume plasmon (1.47, 1.64, and 1.78 eV for ScH_2, YH_2, and LuH_2) and to the onset of interband absorption (see Fig. 5) makes the identification of its origin based only on the thermoreflectance spectra rather difficult. Modeling of the line shape of $\Delta R/R$ can be done in the simplest case where only the contributions arising from the temperature modulation of the broadening parameter and plasma frequency of a Drude gas free of interband absorption need be considered. Such modeling would be less reliable here because of the need to include interband contributions from band states at E_F which may have mixed angular momentum character.

The features in $\Delta R/R$ above ~ 2 eV can be related to interband absorption. Two structures can be seen near 2.5 eV for ScH_2, but in YH_2 the lower-energy one of the pair is very weak (2.45 eV) and it is not observed at all in LuH_2. Each dihydride has a strong minimum near 3.2 eV. The three features at higher energy in ScH_2 and YH_2 are probably of the same origin though the background is different and they have different relative strengths. The energy positions of those structures suggests a widening of the d bands of the hydride for the progression from ScH_2 to LuH_2 since the interband features in YH_2 appear at higher photon energy than in ScH_2 (by ≈ 0.35 eV) and only the first (near 4.4 eV) can be observed in LuH_2. Thermoreflectance measurements above ~ 4.5 eV should reveal the other two features.

Additional insight into the plasmon-interband structure near 1.5–1.8 eV can be gained by considering the temperature induced changes in the dielectric function, $\Delta\epsilon_1$ and $\Delta\epsilon_2$. Those spectra can be determined through Kramers-Kronig analysis of the $\Delta R/R$ results to obtain $\Delta\theta$ and by using the optical constants determined from Fig. 5 for the calculation of the Seraphin coefficients[12] defined as A and B in

$$\Delta\epsilon_1 = \tfrac{1}{2}A\Delta R/R + B\Delta\theta\,, \quad \Delta\epsilon_2 = \tfrac{1}{2}B\Delta R/R - A\Delta\theta,$$

$$A = n(\epsilon_1 - 1) - k\epsilon_2, \quad B = k(\epsilon_1 - 1) + n\epsilon_2. \tag{4}$$

The resulting $\Delta\tilde{\epsilon}$ spectra are shown in Fig. 8. As can be seen, the low-energy region between ~ 1 and ~ 2 eV now has two or three features in $\Delta\epsilon_2$ and corresponding structures in $\Delta\epsilon_1$. The modeling of these structures cannot be done in any straightforward or transparent way. Nevertheless, it is possible to model the temperature modulation of the dielectric function for a free-electron gas by using the linear coefficient of expansion, the temperature coefficient of resistance and the change in temperature at the sample surface. From those calculations, it can be seen that no structure in $\Delta\epsilon_1$ or $\Delta\epsilon_2$ should be expected from a modulation of a free electron gas. Hence, the features shown in Fig. 8 between 1 and 2 eV can be related to interband onset absorption. In the following paper, self-consistent band calculations for ScH_2 and YH_2 will be presented and discussed. The interband structures presented here will be interpreted in some detail based on those energy bands in that paper.

The changes in the volume-loss function induced by temperature modulation, $\Delta\mathrm{Im}(-1/\tilde{\epsilon})$, are shown for ScH_2, YH_2, and LuH_2 in Fig. 9 and were calculated from the results of Fig. 8. The dominant structure occurs in each case near the plasmon

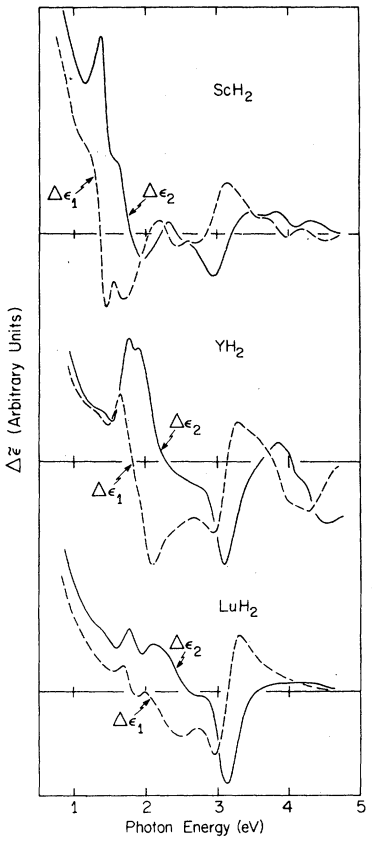

FIG. 8. Temperature dependence of the dielectric function calculated from the thermoreflectance spectra of Fig. 7. The intraband modulation accounts for the monitorically decreasing background below ~ 1.5 eV; interband modulation is responsible for the higher energy features as discussed in detail in Ref. 10.

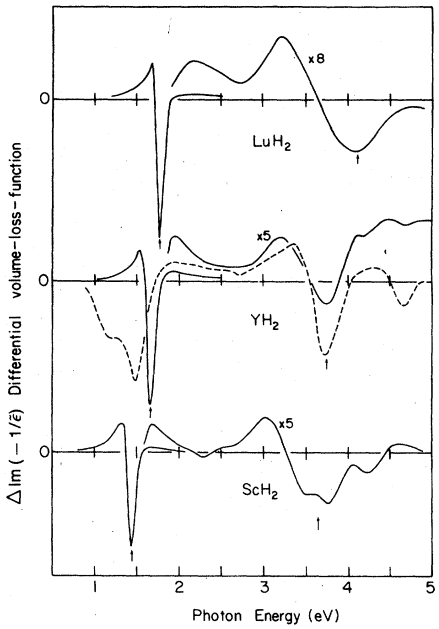

FIG. 9. Differential volume loss function calculated from the results of Fig. 8. The strong feature at lowest energy corresponds to the plasmon with the minimum occurring at the plasma frequency. The higher-energy features are multiplied by the scale factors indicated. The dashed curve for YH_X corresponds to the differential loss function of $YH_{1.96}$ and shows the effects of interband overlap on the plasmon.

frequency. Above 2 eV, the spectra are multiplied by the scale factor shown alongside each curve. The dashed curve for YH_2 represents the differential loss function for the high-concentration $YH_{1.96}$ sample and shows the effects of strong mixing of the "octahedral" interband structure and the volume plasmon. From Fig. 9, we see that the minimum in the differential loss function occurs for $T \simeq 140$ K at 1.79, 1.66, and 1.44 eV for LuH_2, YH_2, and ScH_2, respectively, in agreement with the results of the loss function (Fig. 5).

Some indication of the magnitude of the temperature dependence of the broadening parameter and the plasma frequency can be gained from measurements of $\Delta R/R$ at different temperatures. Our results for LuH_2 at 140 and 340 K show that the width of the $\Delta R/R$ structure (energy separation of the maximum and minimum) increases from 147 meV at 140 K to 174 meV at 340 K. The broadening parameter can be roughly estimated from the zeros of the differential loss function to be 190 meV for 140 K and 220 meV for 340 K. Similarly, the shift in the plasma frequency can be estimated by the shift in the minimum in $\Delta\mathrm{Im}(-1/\tilde{\epsilon})$ from 1.79 eV at 140 K to 1.77 eV at 340 K. Hence, $\Delta\Gamma/\Delta T \approx 1.5\times10^{-4}$ eV/K and $\Delta\omega_p/\Delta T \approx 0.9\times10^{-4}$ eV/K.

VI. SUMMARY

In this paper, we have presented and discussed the results of optical reflectance and thermoreflectance studies of ScH_2, YH_2, and LuH_2 for a range of compositions. We have shown that the low-energy optical properties of YH_x are strongly x dependent with new structures appearing at low energy. These probably have no relation to the energy bands of the dihydride having only tetrahedral hydrogen but instead reflect the effects of octahedral site occupation. Our studies of ScH_x show no analogous interband features and the results are nearly independent of x. The insensitivity of higher energy interband structures in each dihydride suggests that they are due to largely d-derived bands; we have observed no features which showed the strong x dependence that could be attributed to hydrogen-derived band states. The intraband or Drude region has been discussed in detail in this paper and we have sought insight into the low-energy plasmon near 1.5–1.8 eV. Interband structures

have not been interpreted in detail but are deferred until the companion paper for comparison to theory presented therein.

ACKNOWLEDGMENTS

The authors are grateful to many colleagues who contributed to this work. In particular, we thank D. W. Lynch, D. J. Peterman, B. N. Harmon, S. H. Liu, A. C. Switendick, and D. Papaconstantopoulos for many profitable discussions, D. W. Lynch and E. M. Rowe for their continuing support, and H. H. Baker and A. D. Johnson for their expert technical assistance. R. Perry generously provided the vacuum-uv reflectance data used for the Kramers-Kronig analyses. This work has been supported in part by the U. S. Department of Energy, Office of Basic Energy Sciences, Materials Sciences Division, and by the NSF, Division of Materials Research (SRC Contract DMR-77-21888).

---

*Permanent address: Istituto di Fisica "G. Marconi" Universita degli Studi—Roma, Roma, Italy.

[1]T. Graham, Philos. Trans. R. Soc. 156, 415 (1866).

[2]See, for example, F. A. Lewis, *The Palladium-Hydrogen System* (Academic, New York, 1967).

[3]B. Stritzker and W. Buckel, Z. Phys. 257, 1 (1972).

[4]T. Skoskiewicz, Phys. Status Solidi A 11, K123 (1972).

[5]R. J. Miller and C. B. Satterthwaite, Phys. Rev. Lett. 34, 144 (1975).

[6]J. H. Weaver, R. Rosei, and D. T. Peterson, Solid State Commun. 25, 201 (1978).

[7]J. H. Weaver and D. T. Peterson, Phys. Lett A 62, 433 (1977).

[8]A. C. Switendick, Ber. Buns. Phys. Chem. 76, 535 (1972); Solid State Commun. 8, 1463 (1970); J. Less-Common Met. 49, 283 (1976); Int. J. Quantum Chem. 5, 459 (1971).

[9]J. H. Weaver, J. A. Knapp, D. E. Eastman, D. T. Peterson, and C. B. Satterthwaite, Phys. Rev. Lett. 39, 639 (1977).

[10]D. J. Peterman, B. N. Harmon, J. Marchiando, and J. H. Weaver, following paper, Phys. Rev. B 19, 4867 (1979).

[11]See, for example, J. H. Weaver, D. W. Lynch, C. H. Culp, and R. Rosei, Phys. Rev. B 14, 459 (1976); J. H. Weaver, AIP Conf. Proc. 39, 115 (1978).

[12]R. Rosei and D. W. Lynch, Phys. Rev. B 5, 3883 (1972).

[13]D. G. Westlake, C. B. Satterthwaite, and J. H. Weaver, Phys. Today, Nov. 1978, p. 32.

[14]W. M. Mueller, J. P. Blackledge, and G. G. Libowitz, *Metal Hydrides* (Academic, New York, 1968); G. G. Libowitz, *The Solid State Chemistry of Binary Metal Hydrides* (Benjamin, New York, 1965) and references therein.

[15]L. W. Bos and D. W. Lynch, Phys. Rev. B 2, 4567 (1970).

[16]C. D. Gelatt, H. Ehrenreich, and J. A. Weiss, Phys. Rev. B 17, 1940 (1978).

[17]J. H. Weaver and D. T. Peterson, unpublished optical studies of La, Nd, Gd, Tb, Dy, Ho, Er, Tm dihydrides.

[18]J. H. Weaver and C. G. Olson, Phys. Rev. B 16, 731 (1977).

[19]R. Perry generously measured the vacuum-uv reflectance for us.

[20]R. E. Dietz, M. Campagna, J. N. Chazalviel, and H. R. Shanks, Phys. Rev. B 17, 3790 (1978).